

Surface Hopping Excited-State Dynamics Study of the Photoisomerization of a Light-Driven Fluorene Molecular Rotary Motor

Andranik Kazaryan,[†] Zhenggang Lan,[‡] Lars V. Schäfer,[§] Walter Thiel,^{*,‡} and Michael Filatov^{*,||}

[†]Division of Theoretical Chemistry, Vrije Universiteit Amsterdam, De Boelelaan 1083, 1081 HV Amsterdam, The Netherlands

[‡]Max-Planck-Institut für Kohlenforschung, Kaiser-Wilhelm-Platz 1, D-45470, Mülheim an der Ruhr, Germany

[§]Molecular Dynamics, Groningen Biomolecular Sciences and Biotechnology Institute, University of Groningen, Nijenborgh 4, 9747 AG Groningen, The Netherlands

^{||}University of Groningen, Nijenborgh 4, 9747 AG Groningen, The Netherlands

Supporting Information

ABSTRACT: We report a theoretical study of the photoisomerization step in the operating cycle of a prototypical fluorene-based molecular rotary motor (**1**). The potential energy surfaces of the ground electronic state (S_0) and the first singlet excited state (S_1) are explored by semiempirical quantum-chemical calculations using the orthogonalization-corrected OM2 Hamiltonian in combination with a multireference configuration interaction (MRCI) treatment. The OM2/MRCI results for the S_0 and S_1 minima of the relevant **1-P** and **1-M** isomers and for the corresponding S_0 transition state are in good agreement with higher-level calculations, both with regard to geometries and energetics. The S_1 surface is characterized at the OM2/MRCI level by locating two S_0 – S_1 minimum-energy conical intersections and nearby points on the intersection seam and by computing energy profiles for pathways toward these MECIs. Semiclassical Tully-type trajectory surface hopping (TSH) simulations with on-the-fly OM2/MRCI calculations are carried out to study the excited-state dynamics after photoexcitation to the S_1 state. Fast relaxation to the ground state is observed through the conical intersection regions, predominantly through the lowest-energy one with a strongly twisted central C=C double bond and pyramidalized central carbon atom. The excited-state lifetimes for the direct and inverse photoisomerization reactions (1.40 and 1.79 ps) and the photostationary state ratio (2.7:1) from the TSH-OM2 simulations are in good agreement with the available experimental data (ca. 1.7 ps and 3:1). Excited-state lifetimes, photostationary state ratio, and dynamical details of the TSH-OM2 simulations also agree with classical molecular dynamics simulations using a reparametrized optimized potentials for liquid simulations (OPLS) all-atom force field with ad-hoc surface hops at predefined conical intersection points. The latter approach allows for a more extensive statistical sampling.

INTRODUCTION

A design of molecular machines, such as rotary molecular motors and photoswitches, represents a real challenge for future technology.^{1–10} A wide variety of molecular machines ranging from single molecule switches and motors^{5–7,10–22} to photo-mobile polymer materials^{23–25} has been synthesized. The desired functionality, in these machines, is achieved through light-driven changes in molecular structure. This principle is used in light-driven molecular rotary motors derived from chiral overcrowded alkenes^{5–7,12–22} in which periodic repetition of photoisomerization and thermal relaxation steps leads to a unidirectional rotation of one part of the molecule with respect to another (see e.g., Scheme 1). In these motors, clear design principles were formulated for the thermal helix inversion step, and a considerable increase in the rotation speed (ca. 10^8 times) has been achieved by lowering its barrier.^{13,14,16,17} The photoisomerization step however still remained poorly understood and less amenable to judicious chemical modification. To be able to improve the design of light-driven molecular rotary motors, one needs to better understand the underlying mechanism and the effect of various factors, such as substituents, heteroatoms, and environment, on the dynamics of photorearrangement. Such

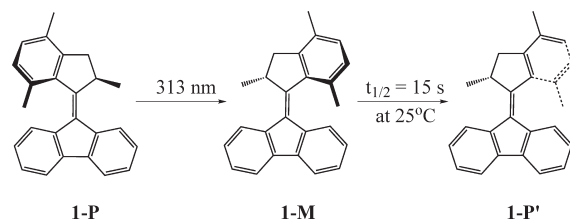
knowledge can be used not only to improve the design of synthetic molecular motors but also to gain deeper insight into the mode of action of biological molecular machines.²⁶

These goals motivated a recent molecular dynamics (MD) study²⁷ of the rotation cycle of a particular molecular motor, 9-(2,4,7-trimethyl-2,3-dihydro-1H-inden-1-ylidene)-9H-fluorene (**1**), see Scheme 1. In this study, the potential energy surfaces (PESs) of the lowest singlet excited state (S_1) and of the electronic ground state (S_0) were represented by a classical force field [optimized potentials for liquid simulations (OPLS) all-atom], with a special parametrization for the excited state.²⁷ The MD-OPLS simulations started in the S_1 state and returned to the S_0 state via conical intersections^{28–30} that play a crucial role in the photoisomerization of **1**. In a general sense, the mechanism of photoisomerization in **1** is basically the same as in the prototypical ethylene molecule. To reach the conical intersection, **1** needs to undergo a substantial geometric distortion that involves a twist about the central double bond and a strong pyramidalization of the central carbon atom of the fluorene moiety. Although

Received: March 23, 2011

Published: May 24, 2011

Scheme 1. Isomerization Cycle of Molecular Motor 1



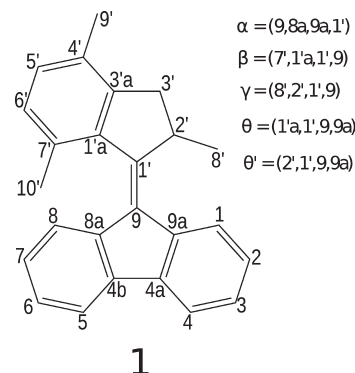
the results of ref 27 for the excited-state lifetimes, the photostationary state ratio, and the thermochemical parameters of the helix inversion step were in good agreement with experiments,¹⁶ the underlying theoretical approach is based on a number of assumptions that could not be thoroughly tested. In particular, it was assumed that the population transfer occurs whenever the molecular conformation reaches a predefined geometry that corresponds to a minimum-energy conical intersection.²⁷ This assumption may artificially exaggerate the role of minimum-energy conical intersections and thus needs to be justified carefully.

A more balanced description of excited-state decay processes can be achieved with the use of semiclassical trajectory surface hopping (TSH) simulations in which the parameters governing population transfer are determined on-the-fly from quantum mechanical (QM) calculations. It is the primary purpose of the present work to carry out such TSH-QM simulations of the photoisomerization cycle of the molecular motor 1 and to obtain detailed insight into its mechanism. The results of this work should not only corroborate those of the previous study²⁷ but also provide an unbiased assessment of the role of conical intersections and avoided crossing regions for the photodynamics of 1. The sheer size of 1 precludes the use of accurate QM methods in on-the-fly TSH-QM simulations. Therefore we have chosen an efficient semiempirical QM approach for this purpose, the OM2/graphical unitary group approach multireference configuration interaction (GUGA-MRCI) method,^{31–33} which offers a realistic description of the ground and excited states of large molecules^{34,35} and has recently been applied successfully in excited-state dynamics studies.^{36–38} In the present TSH-OM2 simulations, we compute the ground- and excited-state PESs of 1 and the required nonadiabatic coupling parameters by OM2/GUGA-MRCI on-the-fly during the dynamics runs. For comparison, we report classical MD-OPLS simulations of the type of ref 27 using the conical intersection seam structures optimized with the OM2/GUGA-MRCI method. We analyze the results of the two types of simulations in the context of the experimentally observed excited-state lifetimes³⁹ and photostationary state ratios¹⁶ and discuss the implications of these results for the photochemistry of sterically overcrowded alkenes.

METHOD OF CALCULATION

To investigate the potential energy surfaces and the dynamics of 1, semiempirical QM calculations were performed using the development version of the MNDO program.⁴⁰ The orthogonalization-corrected OM2 semiempirical Hamiltonian^{31,32} and the GUGA-MRCI approach³³ were employed to calculate the required energies, gradients, and nonadiabatic couplings. GUGA-MRCI denotes the graphical unitary group approach to multireference configuration interaction. Three reference configurations

Scheme 2. Definition of Key Geometric Parameters of 1



[closed-shell and single and double highest occupied–lowest unoccupied molecular orbital (HOMO–LUMO) excitations] were used to build the MRCI expansion. The self-consistent field (SCF) calculations were done in the restricted open-shell Hartree–Fock (ROHF) formalism, which provides a better description of the electronic wave function of singlet excited states than the usual restricted closed-shell Hartree–Fock approach.

The geometries of the ground- and excited-state minima were optimized for all the relevant isomers using the OM2/GUGA-MRCI method. The ground-state transition state (TS) for the first step in Scheme 1 was also optimized at the OM2/GUGA-MRCI level. The geometries of the minimum-energy S_0 – S_1 conical intersections (MECIs) were located by using the Lagrange–Newton method with analytically calculated gradients and nonadiabatic coupling vectors.^{41,42} The conical intersection seam in the vicinity of the located MECIs was studied by performing relaxed scans along dihedral angles corresponding to twisting about the C_9 – $C_{1'}$ double bond and pyramidalization of the C_9 atom (see Scheme 2).

The photoinduced nonadiabatic dynamics was investigated with Tully's surface hopping method (see refs 43–46 for further details). All relevant energies, gradients, and nonadiabatic coupling vectors were calculated on-the-fly using OM2/GUGA-MRCI. Nonadiabatic transitions at conical intersections were treated by the fewest switches algorithm,^{43,44,47} with velocity adjustment along the nonadiabatic coupling vector after a successful hop.⁴⁷ The empirical decoherence correction proposed by Truhlar et al.⁴⁸ and Granucci et al.⁴⁹ was applied to improve the internal consistency of the fewest switches scheme, using the suggested value of 0.1 hartree for the empirical constant in this correction. Initial structures and velocities were obtained by Wigner sampling.⁵⁰ The nuclear trajectories were propagated for 2 ps with a time step of 0.1 fs. A step size of 0.001 fs was used for the propagation of the electronic motion.⁴⁷

The active space in the OM2/GUGA-MRCI calculations comprised 12 electrons in 11 orbitals (π and π^*), which was found suitable for stable dynamics simulations and for geometry optimizations along the isomerization path including the conical intersection points. To always retain the π orbitals in the active space, we employed a recently developed method for identifying and tracking the π character of orbitals.⁵¹ To be included in the active space, a molecular orbital (MO) was required to have a π -type population exceeding 0.4 for optimizations and 0.35 for nonadiabatic dynamics (see ref 51 for further details of this approach). The chosen (12,11) active space contained the two

Table 1. Geometry Parameters in Å and deg of the 1-P and 1-M Conformations, the Transition State, and the Conical Intersections Obtained with OM2/GUGA-MRCI (this work) and with the RE-B3LYP/6-31G* and SA-RE-BH&HLYP//RE-B3LYP/6-31G* Methods (from ref 27)^a

structure(state)	method	C _{1'} –C ₉	α	β	γ	θ	pyr ^b
P(S ₀)	OM2/GUGA-MRCI	1.359	0.7	−39.6	102.2	168.2	1.1
	RE-B3LYP	1.368	1.7	−43.1	105.5	169.2	2.8
M(S ₀)	OM2/GUGA-MRCI	1.364	1.3	27.0	41.2	27.2	2.1
	RE-B3LYP	1.376	1.7	30.0	32.4	31.7	2.8
P(S ₁)	OM2/GUGA-MRCI	1.400	16.4	1.5	59.4	110.2	26.7
M(S ₁)	OM2/GUGA-MRCI	1.392	4.3	0.7	58.6	85.3	6.9
TS(S ₀)	OM2/GUGA-MRCI	1.438	0.2	0.2	59.1	90.0	0.3
	RE-B3LYP	1.463	0.0	5.6	66.0	90.0	0.0
CI ₁	OM2/GUGA-MRCI	1.420	35.5	5.7	67.2	133.5	58.0
	SA-RE-BH&HLYP//RE-B3LYP	1.490	34.0	3.8	36.8	120.0	52.7
	CASSCF(8,8)	1.423	35.5	4.9	64.9	131.0	58.1
CI ₂	OM2/GUGA-MRCI	1.405	−32.6	3.2	59.6	56.1	−53.6
	SA-RE-BH&HLYP//RE-B3LYP	1.472	−30.0	4.9	45.5	70.0	−47.9

^a See Scheme 2 for definitions of geometry parameters for 1-P and 1-M. ^b Pyramidalization angle: angle between C_{1'}–C₉ bond and (8a–9–9a) plane.

Table 2. Energies, in kcal/mol, of the Species in Table 1 Obtained from OM2/GUGA-MRCI (this work) and RE-B3LYP/6-31G* or SA-RE-BH&HLYP/6-31G* (from ref 27) Calculations^a

state	method	P	M	TS	P(S ₁) ^b	M(S ₁) ^c	CI ₁	CI ₂
S ₀	OM2/GUGA-MRCI	0.0	2.1	35.7	40.8	37.8	62.7	66.2
	RE-B3LYP	0.0	3.5	32.1			67.6 ^d	70.3 ^d
S ₁	OM2/GUGA-MRCI	90.6	86.5	62.0	59.1	59.0	62.7	66.2
	SA-RE-BH&HLYP	87.6	81.7	68.0			71.2	74.0

^a All values are given relative to the ground-state energy of the P conformer. ^b Energy minimum on the S₁ PES structurally closest to the 1-P conformer. ^c Energy minimum on the S₁ PES structurally closest to the 1-M conformer. ^d Energy obtained from SA-RE-BH&HLYP//RE-B3LYP single-point calculation.

singly occupied MOs from the ROHF treatment, the 5 highest doubly occupied π MOs, and the 4 lowest unoccupied π MOs, which was considered sufficient for capturing the major correlation effects in the OM2/GUGA-MRCI framework. For this choice, the energy gaps between the active and inactive π MOs were generally rather large, consistent with the fact that the (12,11) active space turned out to be quite robust during dynamics and optimizations.

To verify the molecular geometries obtained at the OM2/GUGA-MRCI level, complete active space SCF (CASSCF) calculations were undertaken for a number of the structures, using an active space with 8 electrons in 8 orbitals and the 6-31G** basis set.⁵² The CASSCF calculations were performed with the MOLPRO2008.1 package.⁵³

The classical force field MD simulations were carried out using the Gromacs (v4.0.5) program package.⁵⁴ The ground- and excited-state potential energy surfaces were described by the OPLS all-atom force field,⁵⁵ as reparametrized in ref 27. Further details on the setup and the results of the classical MD simulations can be found in the Supporting Information. To distinguish in the following between the two types of excited-state dynamics described above, we shall use the label TSH-OM2 for the semiclassical trajectory surface hopping method with on-the-fly OM2/GUGA-MRCI calculations and the label MD-OPLS for the classical MD simulations with the reparametrized OPLS all-atom force field.

RESULTS AND DISCUSSION

OM2/GUGA-MRCI Calculations. The operation cycle of the motor 1 consists of four steps (strokes) of which one photoisomerization step (power stroke) and one thermal helix inversion step are shown in Scheme 1. The geometries of the stable 1-P and the metastable 1-M conformations of 1 in the ground (S₀) electronic state were optimized using the OM2/GUGA-MRCI semiempirical method. The atomic numbering scheme and the definition of the key geometric parameters of 1 are given in Scheme 2, and the results of the calculations are collected in Tables 1 and 2. Due to the increased steric repulsion, the metastable conformation 1-M is destabilized by 2.1 kcal/mol as compared to 1-P, and the central C_{1'}–C₉ bond is elongated by 0.005 Å. These values are in a good agreement with the results of RE-B3LYP/6-31G* calculations ($\Delta E = 3.5$ kcal/mol, $\Delta l = 0.008$ Å) for the ground-state species (see Tables 1 and 2).²⁷ The rearrangement from 1-P to 1-M occurs on the S₀ PES via a transition state that lies 35.7 kcal/mol (OM2/GUGA-MRCI) above the 1-P minimum, see Table 2; the corresponding RE-B3LYP/6-31G* barrier is 32.1 kcal/mol.²⁷ The OM2/GUGA-MRCI transition state possesses an imaginary frequency of 310i cm^{−1} associated with a twist about the C_{1'}–C₉ double bond. Previously, the activation energy of the thermal helix inversion step (second step in Scheme 1) was found^{16,27} to be 18.7 kcal/mol, which guarantees that the helix inversion is the

dominant pathway of relaxation for the metastable conformation **1-M** on the ground-state S_0 PES.

The vertical excitation energies of the stable **1-P** and the metastable **1-M** conformations from OM2/GUGA-MRCI calculations are compared in Table 3 with the results of SA-RE-BH&HLYP//RE-B3LYP and TD-BH&HLYP//B3LYP calculations²⁷ and with the maxima of the absorption bands of the two conformers measured at -40°C in hexane solution.¹⁶ The lowest singlet S_1 excited state corresponds to the excitation of one electron from the π -bonding to the π -antibonding orbital of the central C_1-C_9 double bond. This state is more polar than the ground state, as indicated by the electric dipole moments of the **1-P** and **1-M** conformers in the S_1 and S_0 state, respectively (2.53 vs 1.30 D in **1-P** and 2.25 vs 1.20 D in **1-M**). Due to large values of the transition electric dipole moment, 7.46 D for the **1-P** conformer and 7.43 D for the **1-M** conformer, the S_1 state is

Table 3. Excitation Energies, in eV and in nm (in parentheses), of the Stable Conformers **1-P** and **1-M** Calculated with the OM2/GUGA-MRCI, SA-RE-BH&HLYP, and TD-BH&HLYP Methods

basis set	method	1-P	1-M
6-31G*	OM2/GUGA-MRCI	3.93 (315)	3.75 (331)
	SA-RE-BH&HLYP	3.80 (327)	3.40 (365)
	TD-BH&HLYP	3.78 (328)	3.39 (366)
6-311+G**	SA-RE-BH&HLYP	3.71 (334)	3.31 (375)
	TD-BH&HLYP	3.68 (337)	3.28 (378)
	expt ^a	3.44 (360)	3.22 (385)

^a Maxima of the absorption bands measured in ref 16 in hexane solution at -40°C .

optically accessible, and the **1-P** \rightarrow **1-M** photoisomerization occurs in this state.²⁷ By contrast, the second lowest singlet S_2 excited state is essentially dark. It lies about 0.4 eV above the S_1 state: For the **1-P** conformer, OM2/GUGA-MRCI predicts the S_2 state at 4.31 eV (288 nm) with an oscillator strength of 0.02, compared to the S_1 state at 3.93 eV (315 nm) with an oscillator strength of 0.83.

For illustration purposes, the potential energy surfaces of the S_0 and S_1 states were obtained from relaxed scans on a two-dimensional grid of the dihedral angles θ and α . The positions of the geometric structures listed in Table 1 are shown in Figure 1 by yellow dots located at the respective values of θ and α . The S_1 PES of **1** features an elongated and shallow low-energy region where two nearly degenerate stationary points can be identified. The two structures are denoted in Figure 1 and in Tables 1 and 2 as $P(S_1)$ and $M(S_1)$ based on their geometric proximity to one of the ground-state minima, **1-P** or **1-M**. The $P(S_1)$ minimum lies 31.5 kcal/mol below the Franck–Condon (FC) point corresponding to the **1-P** conformation, and the $M(S_1)$ minimum is 27.5 kcal/mol below the **1-M** FC point. These energy differences suggest that, in the S_1 state, there is a substantial driving force for rotating the upper part of **1** toward twisting angles about the central C_1-C_9 bond of approximately 90° .

The MECI points were located at the OM2/GUGA-MRCI level using the Lagrange–Newton method with analytic non-adiabatic coupling vectors and gradient difference vectors.⁴² The key geometry parameters of these MECI structures and their relative energies are reported in Tables 1 and 2, respectively. In Figure 1, the dihedral angles α and θ corresponding to the optimized MECI structures are shown. Note however that the energies of the optimized MECI points do not exactly match the PES contour plots in this figure (due to differences in the

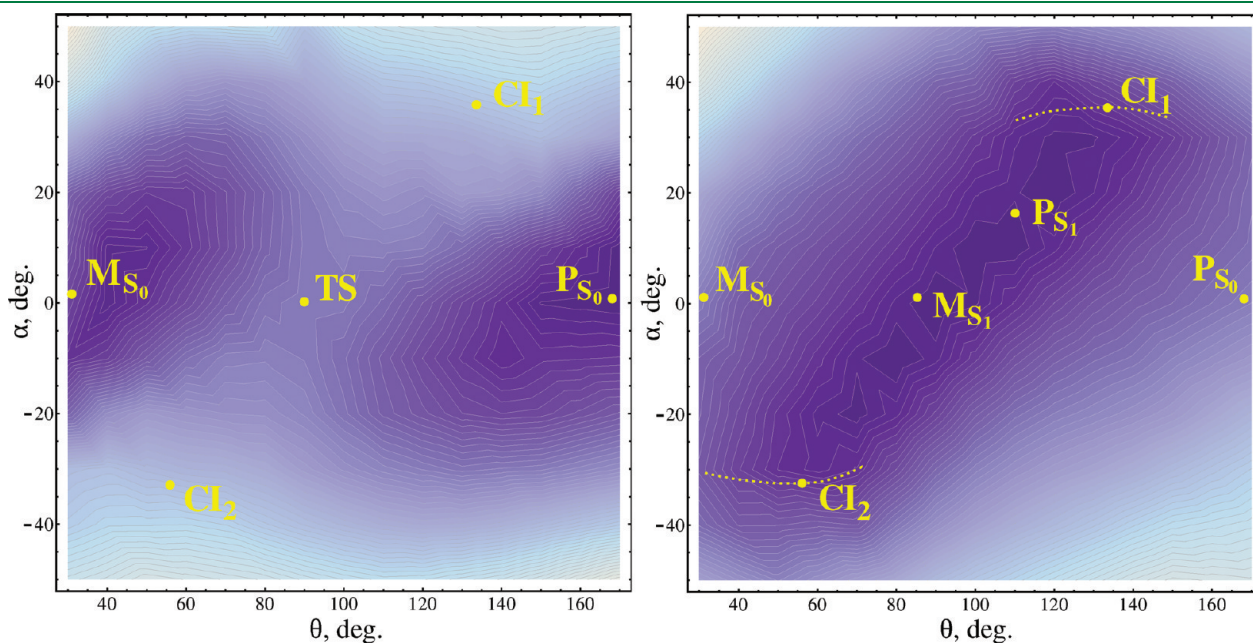


Figure 1. Contour plots of the S_0 and S_1 (right and left panels, respectively) PESs of **1** obtained in OM2/GUGA-MRCI calculations (see text for details). Special points marked on the plots in yellow: P_{S_0} , minimum corresponding to the **1-P** conformation on the S_0 PES; M_{S_0} , minimum corresponding to the **1-M** conformation on the S_0 PES; P_{S_1} , minimum on the S_1 PES geometrically closest to the **1-P** conformation; M_{S_1} , minimum on the S_1 PES geometrically closest to the **1-M** conformation; CI_1 and CI_2 , positions of the two minimum-energy conical intersection points; and TS, transition state on the S_0 PES. Dotted lines on the right panel indicate the positions of the conical intersection seam in the vicinity of MECIs as obtained with the OM2/GUGA-MRCI method.

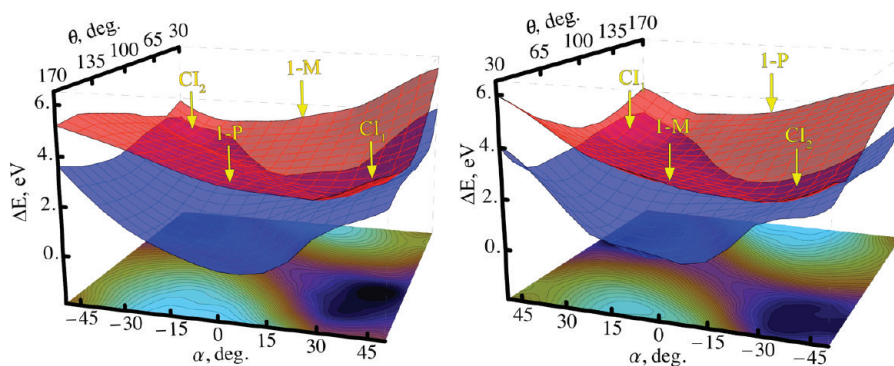


Figure 2. Profiles of the S_0 (blue) and S_1 (red) PESs of **1** obtained from OM2/GUGA-MRCI calculations (see text for details). Left panel: view from the side of the 1-P conformation. Right panel: view from the side of the 1-M conformation. The positions of conical intersection points and Franck–Condon points are shown with yellow arrows. The contour plots below show the difference between the S_1 and S_0 energies.

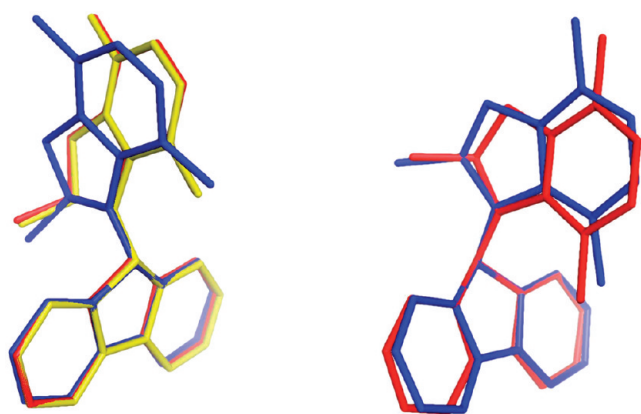


Figure 3. CI_1 and CI_2 (left and right panels, respectively) structures as obtained from OM2/GUGA-MRCI (red), RE-BH&HLYP/6-31G* (blue) and CASSCF(8,8)/6-31G* (yellow) calculations (see text for details).

other geometrical parameters). The two MECIs denoted as CI_1 and CI_2 feature pronounced pyramidalization of the C_9 atom and lie on the opposite sides of the avoided crossing region, i.e., the region in the vicinity of the TS on the S_0 PES, see Figures 1 and 2. Similar conical intersection geometries were obtained previously by Kazaryan et al.²⁷ using the SA-RE-BH&HLYP/6-31G* method. Note however that there was no search to precisely locate the MECI points in ref 27. Nevertheless, the geometries of the CI_1 and CI_2 points from the present work and from ref 27 closely coincide, as can be seen in Figure 3 where molecular drawings of the CI_1 and CI_2 geometries are superimposed. For comparison, a geometry optimized for the CI_1 point using the CASSCF(8,8) method is also shown in Figure 3.

Energetically CI_1 and CI_2 lie 3–5 kcal/mol above the P_{S1} and M_{S1} minima on the S_1 PES of **1**. The CI_1 point is easily accessible from the respective FC points of the 1-P and 1-M conformations (see Figure 4), whereas there is a small barrier (ca. 3.8 kcal/mol) en route from 1-M to CI_1 . This is illustrated in Figure 4 where the PES profiles are shown along pathways connecting the following points on the S_0 and S_1 surfaces: 1-P, P_{S1} , CI_1 , and 1-M; 1-P, P_{S1} , CI_2 , and 1-M; 1-P, CI_1 , M_{S1} , and 1-M; and 1-P, CI_2 , M_{S1} , and 1-M. These PES profiles were obtained by performing relaxed scans in these directions. During the scans, constrained geometry optimizations were carried out in the S_1 state for the intervals

shown in Figure 4 with solid red lines, for fixed values of the dihedral angles θ and α that were obtained by linear interpolation between the respective structures; the S_0 energies (dashed blue lines) were then computed at these optimized S_1 geometries. After reaching a conical intersection, it was assumed that the system switches to the S_0 ground state. Therefore constrained ground-state geometry optimizations were carried out for the intervals shown in Figure 4 with solid blue lines; the S_1 energies (dashed red lines) were obtained from single-point calculations at the S_0 geometries. The resulting PES profiles are presented in Figure 4.

It is well-known that conical intersections play a crucial role in the radiationless relaxation of excited states.^{28–30} The computed PES profiles of **1** suggest that the photoisomerization reaction can proceed via a barrierless pathway, and the expected excited-state lifetime should thus be quite short, of the order of 1 ps.³⁰ Specifically, for 1-P, the energy profiles for the S_1 state indicate that the relaxation should predominantly occur via CI_1 (see Figure 4), which is more easily accessible and also lower in energy than CI_2 (see Table 2). We note that barrierless pathways toward conical intersection points were recently also reported for a molecular switch structurally similar to **1**.^{21,22} However, even if such favorable pathways exist, the actual trajectories on the S_1 PES may take somewhat different routes due to dynamical effects. To obtain more realistic information on the dynamical behavior of the system after photoexcitation and on experimental observables, such as the quantum yields of photoisomerization, one needs to carry out excited-state dynamics simulations starting from the respective FC regions.

Molecular Dynamics Simulations. In our semiempirical TSH-OM2 simulations, 120 trajectories were initiated for each of the 1-P \rightarrow 1-M and 1-M \rightarrow 1-P photoisomerization reactions. The simulations were started in the S_1 state at geometries in the vicinity of the respective FC point, and the nuclear trajectories were propagated for 2 ps. The populations of the S_0 and S_1 states averaged over all trajectories are shown in Figure 5 for the two reactions. The S_1 populations were fitted by an exponential function, which gave S_1 lifetimes of 1.40 and 1.79 ps for the 1-P \rightarrow 1-M and 1-M \rightarrow 1-P reactions, respectively. These values are in a good agreement with the lifetimes of 1.40 ± 0.10 and 1.77 ± 0.13 ps, respectively, reported previously by Kazaryan et al. in their first classical MD-OPLS simulations.²⁷

To gain more detailed structural insight into the radiationless relaxation from S_1 to S_0 , we inspect some characteristic angles in

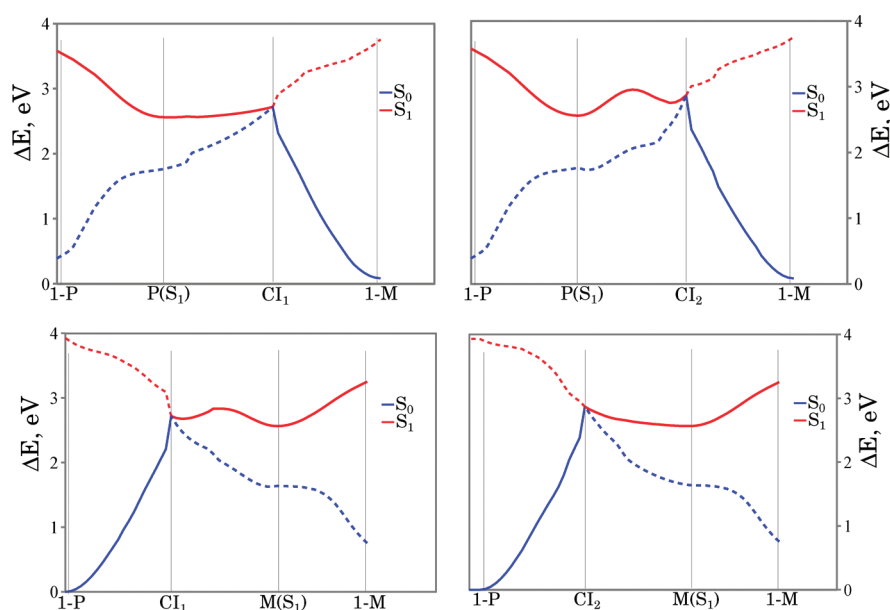


Figure 4. PES profiles connecting the 1-P, P_{S1} , CI_1 , and 1-M structures (upper left panel), the 1-P, P_{S1} , CI_2 , and 1-M structures (upper right panel), the 1-P, CI_1 , M_{S1} , and 1-M structures (lower left panel), and the 1-P, CI_2 , M_{S1} , and 1-M structures (lower right panel) on the S_1 (red) and S_0 (blue) PES. The solid lines represent energies obtained from constrained geometry optimization in the respective electronic state, and the dashed lines refer to energies obtained in single-point calculations (see text for further details).

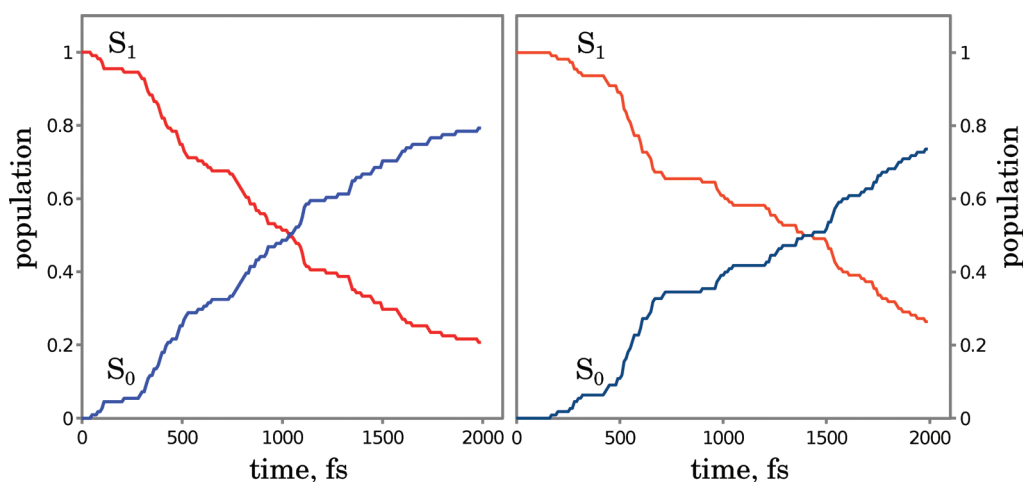


Figure 5. Populations of the S_0 (blue) and S_1 (red) states as a function of time (in fs) for the 1-P \rightarrow 1-M (left panel) and 1-M \rightarrow 1-P (right panel) photoisomerization reactions as obtained from the TSH-OM2 simulations.

the geometries at which surface hops occur during the TSH-OM2 simulations. The histograms in Figure 6 show the probability of surface hops as a function of the absolute values of the twisting angle θ and the pyramidalization angles at the C_9 atom and the $C_{1'}$ atom, for all trajectories generated for the two photoisomerization reactions. Obviously, the surface hops take place predominantly at sufficiently large values of θ (ca. 110° on average) and $\text{pyr-}C_9$ (ca. 35° on average). The $C_{1'}$ atom remains in a practically planar environment. It can therefore be conjectured that the surface hops occur in the vicinity of one of the MECIs found in the preceding OM2/GUGA-MRCI geometry optimizations. Indeed, both MECIs feature a rather strongly pyramidalized C_9 atom and a substantial twist about the $C_9-C_{1'}$ bond. The large average value of the dihedral angle θ also

suggests that, for both photoisomerization reactions, the hops occur predominantly close to the CI_1 geometry (see Table 1). These findings are consistent with the assumptions made in ref 27 when setting up the classical MD simulations.

More detailed information on the populations of the various molecular structures in the S_0 and S_1 states is presented in Figure 7, where the following distinctions are made in the analysis of the TSH-OM2 trajectories: The $P(S_0)$ structure corresponds to all molecular geometries with $\theta \geq 120^\circ$ encountered on the S_0 PES. The $P(S_1)$ structure corresponds to all geometries with $\theta \geq 120^\circ$ encountered on the S_1 PES. Analogous definitions hold for the $M(S_0)$ and $M(S_1)$ structures with $\theta \leq 70^\circ$. The $X(S_0)$ and $X(S_1)$ structures correspond to all intermediate geometries in the S_0 and S_1 states. These plots

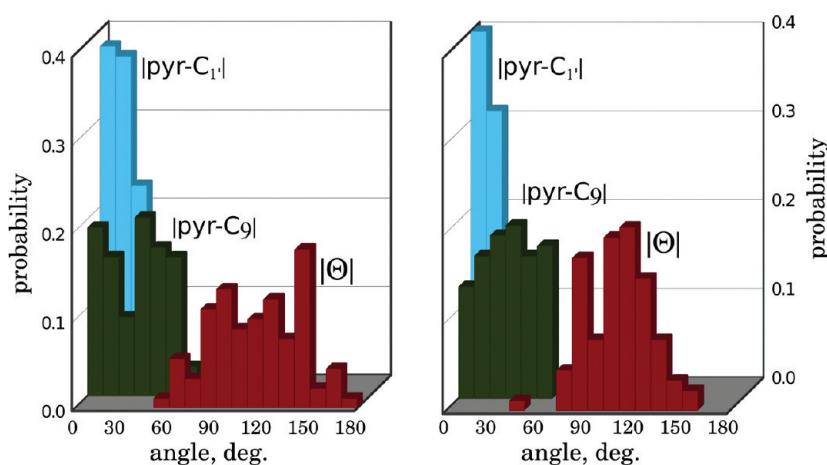


Figure 6. Probability of surface hops as a function of the absolute value of the angles θ (red), pyr-C₉ (green), and pyr-C_{1'} (light blue) in the TSH-OM2 trajectories for the 1-P \rightarrow 1-M (left panel) and 1-M \rightarrow 1-P (right panel) photoisomerization reactions. See Scheme 2 for the definition of θ and atom labels; pyr-C₉ is the angle between C₉–C_{1'} bond and (8a–9–9a) plane; and pyr-C_{1'} is the angle between C₉–C_{1'} bond and (1'a–1'–2') plane.

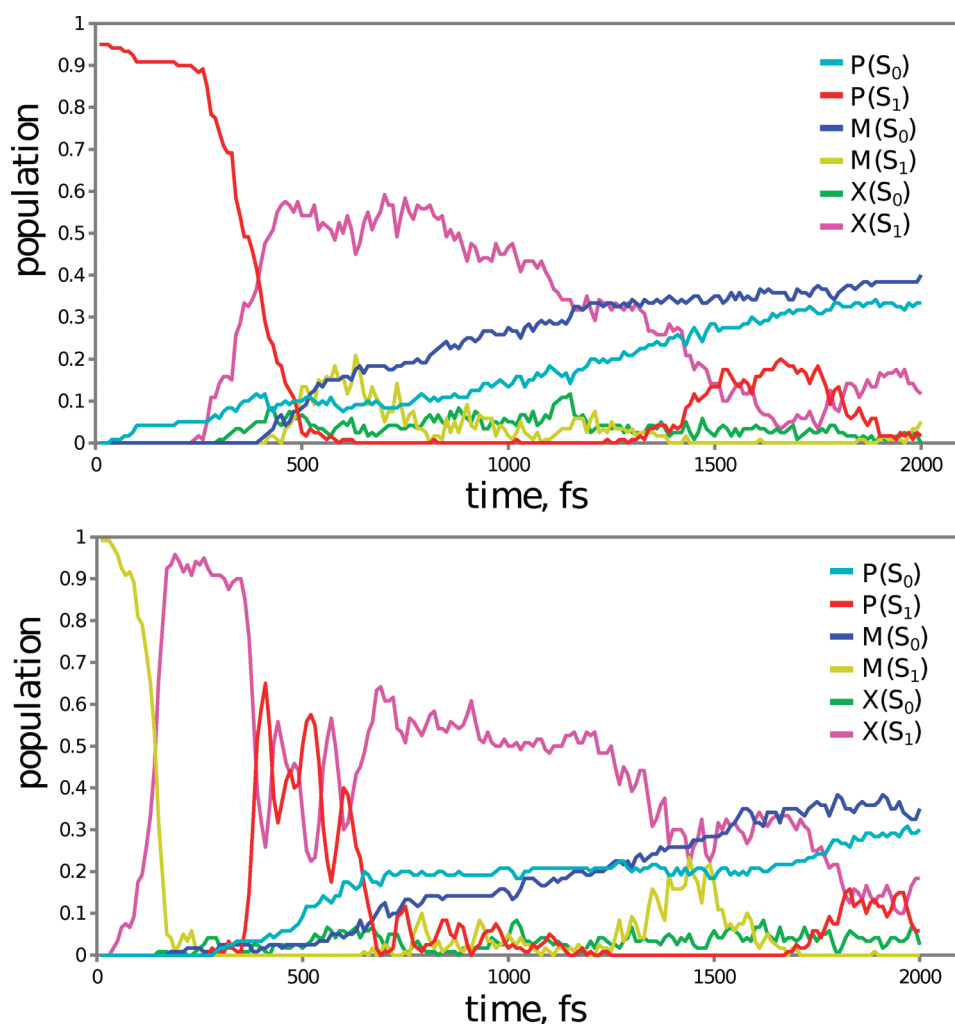


Figure 7. Time evolution of the populations of 1-P and 1-M structures in the ground S_0 and excited S_1 states as obtained from the TSH-OM2 simulations of the 1-P \rightarrow 1-M (upper panel) and 1-M \rightarrow 1-P (lower panel) photoisomerization reactions. Notation: P(S_0), 1-P isomer in the ground state; P(S_1), 1-P isomer in the excited state; M(S_0), 1-M isomer in the ground state; M(S_1), 1-M isomer in the excited state; X(S_0), intermediate molecular structure in the ground state; and X(S_1), intermediate molecular structure in the excited state (see text for details).

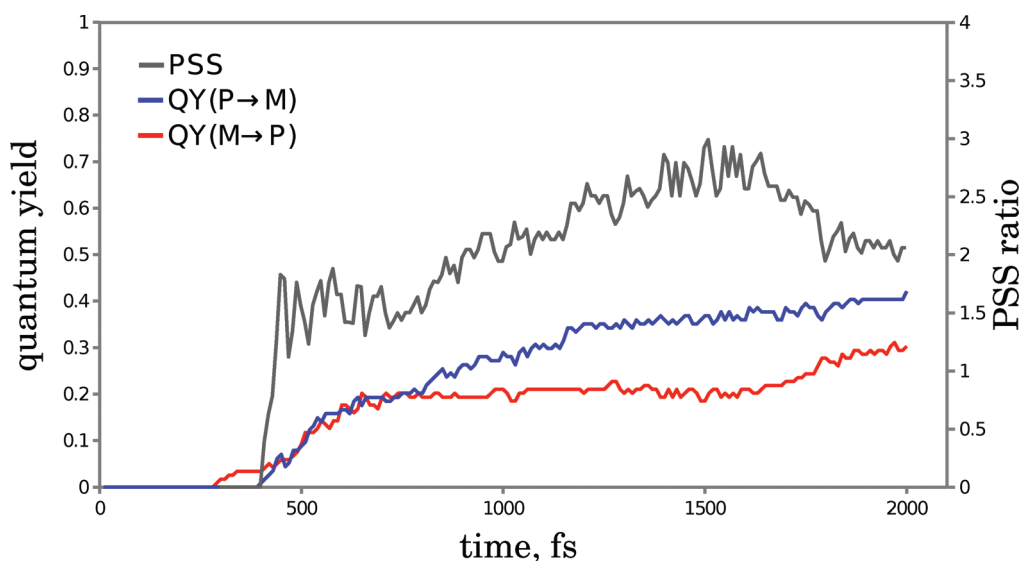


Figure 8. Quantum yields of the $1\text{-P} \rightarrow 1\text{-M}$ (blue) and $1\text{-M} \rightarrow 1\text{-P}$ (red) photoisomerization reactions and photostationary state ratio (gray) of the $1\text{-P} \rightleftharpoons 1\text{-M}$ photoisomerization reaction as obtained from the TSH-OM2 simulations.

indicate that the $1\text{-P} \rightarrow 1\text{-M}$ photoisomerization reaction is practically finished after ca. 1.5 ps, with less than 20% of the trajectories remaining in the excited state near the 1-P geometry. In the case of the $1\text{-M} \rightarrow 1\text{-P}$ reaction, ca. 30% of the trajectories remain in the excited state after ca. 1.6 ps, with the geometries intermediate between the 1-P and 1-M structures. This is as expected from the lifetimes evaluated for the two reactions from the data in Figure 5. We refrain from analyzing the data beyond 1.5 ps because of technical difficulties. In TSH-OM2 runs, the identification of active orbitals and the tracking of the active space may become problematic at longer simulation times, which may result in discontinuous PESs and unphysically large energy gradients.⁵¹ While these problems may be partly overcome by the techniques proposed previously⁵¹ and applied presently, they became unacceptably large for some of the trajectories after propagation times of more than 1.6 ps so that we prefer to focus on the TSH-OM2 results up to 1.5 ps.

In spite of these technical difficulties, we may still estimate the quantum yields of the two photoisomerization reactions and the photostationary state (PSS) ratio from Figure 7. The isomerization quantum yield of $1\text{-P} \rightarrow 1\text{-M}$ can be obtained as the ratio of the population of the $M(S_0)$ structures to the overall population of all structures at the start of the trajectories. The quantum yield of $1\text{-M} \rightarrow 1\text{-P}$ can be defined analogously using the $P(S_0)$ population. The PSS ratio of the $1\text{-P} \rightleftharpoons 1\text{-M}$ photoisomerization reaction is then defined as the ratio of the two quantum yields. To make the calculated PSS ratio comparable to the experimentally measured one, the ratio of quantum yields was multiplied by the ratio of the optical absorption cross sections of the two conformers, 1-P and 1-M ,²⁷ which amounts to 1.5:1.¹⁶ The so-obtained quantum yields and the PSS ratio are shown in Figure 8 as a function of simulation time. It is seen that, between 1.4 and 1.6 ps, the PSS ratio runs into a plateau and then suddenly decreases. Because this decrease is due to technical issues (see above), the final value of the PSS ratio was evaluated as the average value over the interval between 1.4 and 1.6 ps, which yields a value of 2.7:1 in a good agreement with the experimentally measured value of ca. 3:1.¹⁶ Please note that the computed value refers to the gas phase, while the experimental value was determined in perdeuterated toluene.¹⁶

The simulation times that can be achieved in the TSH-OM2 simulations are rather short. To investigate whether the equilibrium parameters derived from the TSH-OM2 simulations are reliable, we used classical two-state MD-OPLS simulations, as outlined in ref 27. We initiated 1000 MD simulations in the 1-P and 1-M states, respectively, and the simulations were run for up to 10 ps, which allowed us to determine converged equilibrium parameters.

A detailed account of the setup and the results of the MD-OPLS simulations is given in the Supporting Information. In the present work, we extended our MD-OPLS approach of ref 27 toward a more detailed description of the CI seam, which is represented by a number of conical intersection points around the two MECIs optimized with OM2/GUGA-MRCI (see Figure 1 in this article and Table 1 in the Supporting Information). In spite of the quite different approaches, the time evolution of the total population of the S_0 and the S_1 states as well as the populations of individual species on the excited- and ground-state PESs of the $1\text{-P} \rightarrow 1\text{-M}$ and $1\text{-M} \rightarrow 1\text{-P}$ photoisomerization reactions obtained in the classical MD-OPLS simulations (see Figures 1 and 2 of the Supporting Information) closely match those from the TSH-OM2 simulations (see Figure 5). The equilibrium values of isomerization quantum yields are reached after ca. 2.5 ps (Figure 3 of Supporting Information). The value of the PSS ratio at ca. 1.5 ps is not very different from the converged value, thus justifying the approach used to calculate the PSS ratio from the results of the TSH-OM2 simulations (see Figure 8).

In summary, the dynamics of the photoisomerization obtained in the TSH-OM2 simulations is consistent with previous theoretical results²⁷ and with the available experimental data.¹⁶ Comparing results of the present work with theoretical work on other photoactive molecules, the character of the lowest excited states and the mechanism of photoisomerization are qualitatively similar to what has been reported for stilbene,^{56–58} which is not too surprising since the molecular rotor **1** contains the stilbene substructure and may be regarded as some kind of stiff stilbene.⁵⁸ Like in ethylene and stilbene, the relevant conical intersection is characterized by a twist about the central double bond and a strong pyramidalization at one of its two carbon

atoms. The radiationless relaxation to the ground state is an ultrafast subpicosecond process in ethylene and stilbene; it is still fast in our case, with an excited-state lifetime of 1.4 ps for 1-P, albeit clearly slower than in ethylene and stilbene. Qualitatively, this may be due to the stiffness of 1 (arising from the annelated rings at both sides of the central double bond), which should make it more difficult to reach the conical intersection region with one strongly pyramidalized carbon atom. Finally, we note that other types of conical intersections have been reported to be involved in the photoisomerization of longer polyenes^{59,60} and of protonated or alkylated Schiff bases that serve as retinal models⁶¹ or molecular switches.²¹

CONCLUSIONS

In this work, we report the results of semiclassical TSH-OM2 and classical MD-OPLS simulations of the photoisomerization step in the rotational cycle of the fluorene-based molecular rotary motor 1. In such motors based on overcrowded alkenes, unidirectional rotation is achieved due to periodic repetition of photoisomerization and thermal relaxation steps. Hitherto, clear design principles were formulated for the thermally activated helix inversion step,^{13,14,16} whereas the photoisomerization step remained poorly understood and less amenable to rational modification based on mechanistic understanding. A first attempt to reach such an understanding was made in ref 27 using classical two-state MD simulations for 1 with a reparametrized all-atom force field. Although the results obtained were in good agreement with experiment, the chosen ad-hoc approach was based on a number of assumptions, the validity of which could not be thoroughly tested.

The present work extends the previous study²⁷ in several ways. First, the use of the OM2/GUGA-MRCI method allows a comprehensive investigation of the excited-state dynamics. A thorough characterization of the excited-state PES of 1 has been achieved for the first time, which provides information on the topology of the conical intersection seam, the location of the energy minima, and the potential energy barriers. On the relaxed PES, the conical intersection seam is found to be easily accessible, without the need to cross potential energy barriers. This observation suggests a reinterpretation of the results of transient absorption experiments in hexane,³⁹ in which a short excited-state decay time (ca. 1.7 ps) was interpreted as relaxation time due to crossing a potential barrier. The S_1 decay times obtained in the present gas-phase work from the TSH-OM2 simulations ($\tau_{S_1} \approx 1.40$ – 1.79 ps), as well as those from ref 27 ($\tau_{S_1} \approx 1.40$ – 1.77 ps), indicate that this relaxation time should be interpreted as excited-state lifetime. The other experimentally observed decay time, ca. 12 ps, which was associated with the transfer of population from the excited to the ground state,³⁹ may actually correspond to vibrational cooling of the “hot” ground-state species.

The semiclassical TSH-OM2 simulations clearly show that the radiationless relaxation of the excited electronic state of 1 proceeds via the conical intersection seam and that other parts of the excited state PES do not play a significant role in the mechanism of photoisomerization. Previously, this was only guessed.²⁷ The computed excited-state lifetimes for the direct, 1-P \rightarrow 1-M, and inverse, 1-M \rightarrow 1-P, photoisomerization reactions and the photostationary state ratio from the TSH-OM2 simulations are in good agreement with previous work²⁷ and with the experimental measurements.^{16,39}

The detailed knowledge of the excited-state PES profiles and of the geometries on the conical intersection seam obtained from OM2/GUGA-MRCI calculations allowed us to amend the approach used in ref 27 and to run classical MD-OPLS simulations using an extended conical intersection seam. The excited-state lifetimes, the detailed dynamics of various conformations, and the photostationary state ratio are in good agreement with the TSH-OM2 results. After proper validation, such excited-state classical MD simulations, with predefined conical intersection structures for hopping to the ground state, can thus be useful for running very long simulations (of the order of 10 ps or more) to reach converged results or for quickly exploring the excited-state dynamics of very large molecular species. A possible application would be to study the effect of chemical modifications on the photoisomerization cycle of rotary molecular motors.

ASSOCIATED CONTENT

S Supporting Information. The setup and the results of the classical MD simulations. This material is available free of charge via the Internet at <http://pubs.acs.org>.

AUTHOR INFORMATION

Corresponding Author

*E-mail: thiel@mpi-muelheim.mpg.de; m.filatov@rug.nl.

ACKNOWLEDGMENT

Z.L. and W.T. are grateful for financial support from Volkswagenstiftung. L.V.S. thanks The Netherlands Organization for Scientific Research (NWO) for a Veni fellowship (700.57.404).

REFERENCES

- (1) Stoddart, J. F. Molecular machines. *Acc. Chem. Res.* **2001**, *34*, 410–411.
- (2) Kottas, G. S.; Clarke, L. I.; Horinek, D.; Michl, J. Artificial Molecular Rotors. *Chem. Rev.* **2005**, *105*, 1281–1376.
- (3) Balzani, V.; Venturi, M.; Credi, A. *Molecular devices and machines, a journey into the nanoworld*; Wiley-VCH: Weinheim, Germany, 2003.
- (4) *Molecular Switches*; Feringa, B. L., Ed.; Wiley-VCH: Weinheim, Germany, 2001.
- (5) Feringa, B. L. In Control of Motion: From Molecular Switches to Molecular Motors. *Acc. Chem. Res.* **2001**, *34*, 504–513.
- (6) Browne, W. R.; Feringa, B. L. Making Molecular Machines Work. *Nat. Nanotechnol.* **2006**, *1*, 25–35.
- (7) Feringa, B. L. The Art of Building Small: From Molecular Switches to Molecular Motors. *J. Org. Chem.* **2007**, *72*, 6635–6652.
- (8) Kay, E. R.; Leigh, D. A.; Zerbetto, F. Synthetic Molecular Motors and Mechanical Machines. *Angew. Chem., Int. Ed.* **2007**, *46*, 72–191.
- (9) Irie, M. Photochromism and molecular mechanical devices. *Bull. Chem. Soc. Jpn.* **2008**, *81*, 917–926.
- (10) Balzani, V.; Credi, A.; Venturi, M. Light powered molecular machines. *Chem. Soc. Rev.* **2009**, *38*, 1542–1550.
- (11) Comstock, M. J.; Levy, N.; Kirakosian, A.; Cho, J.; Lauterwasser, F.; Harvey, J. H.; Strubbe, D. A.; Fréchet, J. M. J.; Trauner, D.; Louie, S. G.; Crommie, M. F. Reversible Photomechanical Switching of Individual Engineered Molecules at a Metallic Surface. *Phys. Rev. Lett.* **2007**, *99*, 038301+.
- (12) Koumura, N.; Zijlstra, R. W. J.; van Delden, R. A.; Harada, N.; Feringa, B. L. Light-driven monodirectional molecular rotor. *Nature* **1999**, *401*, 152–155.
- (13) Koumura, N.; Geertsema, E. M.; van Gelder, M. B.; Meetsma, A.; Feringa, B. L. Second Generation Light-Driven Molecular Motors.

Unidirectional Rotation Controlled by a Single Stereogenic Center with Near-Perfect Photoequilibria and Acceleration of the Speed of Rotation by Structural Modification. *J. Am. Chem. Soc.* **2002**, *124*, 5037–5051.

(14) Pijper, D.; van Delden, R. A.; Meetsma, A.; Feringa, B. L. Acceleration of a Nanomotor: Electronic Control of the Rotary Speed of a Light-Driven Molecular Rotor. *J. Am. Chem. Soc.* **2005**, *127*, 17612–17613.

(15) van Delden, R. A.; ter Wiel, M. K. J.; Pollard, J., M. M.; Vicario; Koumura, N.; Feringa, B. L. Unidirectional molecular motor on a gold surface. *Nature* **2005**, *437*, 1337–1340.

(16) Pollard, M. M.; Meetsma, A.; Feringa, B. L. A redesign of light-driven rotary molecular motor. *Org. Biomol. Chem.* **2008**, *6*, 507–512.

(17) Klok, M.; Boyle, N.; Pryce, A., M. T.; Meetsma; Browne, W. R.; Feringa, B. L. MHz unidirectional rotation of molecular rotary motors. *J. Am. Chem. Soc.* **2008**, *130*, 10484–10485.

(18) London, G.; Carroll, G. T.; Fernández Landaluce, T.; Pollard, M. M.; Rudolf, P.; Feringa, B. L. Light-driven altitudinal molecular motors on surfaces. *Chem. Commun.* **2009**, 1712–1714.

(19) Browne, W. R.; Feringa, B. L. Light Switching of Molecules on Surfaces. *Annu. Rev. Phys. Chem.* **2009**, *60*, 407–428.

(20) Geertsma, E. M.; van der Molen, S. J.; Martens, M.; Feringa, B. L. MHz unidirectional rotation of molecular rotary motors. *Proc. Natl. Acad. Sci. U.S.A.* **2009**, *106*, 16919–16924.

(21) Sinicropi, A.; et al. An artificial molecular switch that mimics the visual pigment and completes its photocycle in picoseconds. *Proc. Natl. Acad. Sci. U.S.A.* **2008**, *105*, 17642–17647.

(22) Rivado-Casas, L.; Sampedro, D.; Campos, P. J.; Fusi, S.; Zanirato, V.; Olivucci, M. Fluorenylidene-Pyrroline Biomimetic Light-Driven Molecular Switches. *J. Org. Chem.* **2009**, *74*, 4666–4674.

(23) Yu, Y.; Nakano, M.; Ikeda, T. Directed Bending of A Polymer Film by Light. *Nature* **2003**, *425*, 145.

(24) Yamada, M.; Kondo, M.; Mamiya, J.-I.; Yu, Y.; Kinoshita, M.; Barrett, C.-J.; Ikeda, T. Photomobile Polymer Materials: Towards Light-Driven Plastic Motors. *Angew. Chem., Int. Ed.* **2008**, *47*, 4986–4988.

(25) Naka, Y.; Mamiya, J.-I.; Shishido, A.; Washio, M.; Ikeda, T. Direct fabrication of photomobile polymer materials with an adhesive-free bilayer structure by electron-beam irradiation. *J. Mater. Chem.* **2011**, *21*, 1681–1683.

(26) Strambi, A.; Durbecja, B.; Ferré, N.; Olivucci, M. Anabaena sensory rhodopsin is a light-driven unidirectional rotor. *Proc. Natl. Acad. Sci. U.S.A.* **2010**, *107*, 21322–21326.

(27) Kazaryan, A.; Kistemaker, J. C. M.; Schäfer, L. V.; Browne, W. R.; Feringa, B. L.; Filatov, M. Understanding the Dynamics Behind the Photoisomerization of a Light-Driven Fluorene Molecular Rotary Motor. *J. Phys. Chem. A* **2010**, *114*, 5058–5067.

(28) Yarkony, D. R. Diabolical Conical Intersections. *Rev. Mod. Phys.* **1996**, *68*, 985–1013.

(29) Bernardi, F.; Olivucci, M.; Robb, M. A. Potential energy surface crossings in organic photochemistry. *Chem. Soc. Rev.* **1996**, *25*, 321–328.

(30) Levine, B. G.; Martinez, T. J. Isomerization Through Conical Intersections. *Annu. Rev. Phys. Chem.* **2007**, *58*, 613–634.

(31) Weber, W. Ph.D. Thesis; Universität Zürich: Zürich, Switzerland, 1996.

(32) Weber, W.; Thiel, W. Orthogonalization corrections for semiempirical methods. *Theor. Chem. Acc.* **2000**, *103*, 495–506.

(33) Koslowski, A.; Beck, M. E.; Thiel, W. Implementation of a general multireference configuration interaction procedure with analytic gradients in a semiempirical context using the graphical unitary group approach. *J. Comput. Chem.* **2003**, *24*, 714–726.

(34) Otte, N.; Scholten, M.; Thiel, W. Looking at Self-Consistent-Charge Density Functional Tight Binding from a Semiempirical Perspective. *J. Phys. Chem. A* **2007**, *111*, 5751–5755.

(35) Silva-Junior, M. R.; Thiel, W. Benchmark of Electronically Excited States for Semiempirical Methods: MNDO, AM1, PM3, OM1, OM2, OM3, INDO/S and INDO/S2. *J. Chem. Theory Comput.* **2010**, *6*, 1546–1564.

(36) Fabiano, E.; Thiel, W. Nonradiative deexcitation dynamics of 9H-adenine: An OM2 surface hopping study. *J. Phys. Chem. A* **2008**, *112*, 6859–6863.

(37) Lan, Z.; Fabiano, E.; Thiel, W. Photoinduced Nonadiabatic Dynamics of 9H-Guanine. *ChemPhysChem* **2009**, *10*, 1225–1229.

(38) Lan, Z.; Fabiano, E.; Thiel, W. Photoinduced Nonadiabatic Dynamics of Pyrimidine Nucleobases: On-the-Fly Surface-Hopping Study with Semiempirical Methods. *J. Phys. Chem. B* **2009**, *11*, 3548–3555.

(39) Augulis, R.; Klok, M.; Feringa, B. L.; van Loosdrecht, P. H. M. Light-Driven Rotary Molecular Motors: an Ultrafast Optical Study. *Phys. Status Solidi C* **2009**, *6*, 181–184.

(40) Thiel, W. MNDO program, version 6.1; Max-Planck-Institut für Kohlenforschung: Mülheim, 2007.

(41) Domcke, W.; Yarkony, D. R.; Köppel, H. *Conical Intersections: Electronic Structure, Dynamics and Spectroscopy*; World Scientific: Singapore, 2004.

(42) Keal, T. W.; Koslowski, A.; Thiel, W. Comparison of algorithms for conical intersection optimization using semiempirical methods. *Theor. Chem. Acc.* **2007**, *118*, 837–844.

(43) Tully, J. C. Molecular dynamics with electronic transitions. *J. Chem. Phys.* **1990**, *93*, 1061–1071.

(44) Hammes-Schiffer, S.; Tully, J. C. Proton transfer in solution: Molecular dynamics with quantum transitions. *J. Chem. Phys.* **1994**, *101*, 4657–4667.

(45) Barbatti, M.; Granucci, G.; Persico, M.; Ruckebauer, M.; Vazdar, M.; Eckert-Maksić, M.; Lischka, H. *J. Photochem. Photobiol. A* **2007**, *190*, 228–240.

(46) Fabiano, E.; Groenhof, G.; Thiel, W. Approximate switching algorithms for trajectory surface hopping. *Chem. Phys.* **2008**, *351*, 111–116.

(47) Fabiano, E.; Keal, T. W.; Thiel, W. Implementation of surface hopping molecular dynamics using semiempirical methods. *Chem. Phys.* **2008**, *349*, 334–347.

(48) Zhu, C.; Jasper, A. W.; Truhlar, D. G. Non-Born-Oppenheimer Liouville-von Neumann Dynamics. Evolution of a Subsystem Controlled by Linear and Population-Driven Decay of Mixing with Decoherent and Coherent Switching. *J. Chem. Theory Comput.* **2005**, *1*, 527–540.

(49) Granucci, G.; Persico, M.; Zocante, A. Including quantum decoherence in surface hopping. *J. Chem. Phys.* **2010**, *133*, 134111+.

(50) Wigner, E. On the Quantum Correction For Thermodynamic Equilibrium. *Phys. Rev.* **1932**, *40*, 749–759.

(51) Keal, T. W.; Wanko, M.; Thiel, W. Assessment of semiempirical methods for the photoisomerisation of a protonated Schiff base. *Theor. Chem. Acc.* **2009**, *123*, 145–156.

(52) Krishnan, R.; Binkley, J. S.; Seeger, R.; Pople, J. A. Self-consistent molecular orbital methods. XX. A basis set for correlated wave functions. *J. Chem. Phys.* **1980**, *72*, 650–654.

(53) Werner, H.-J.; Knowles, P. J. et al. MOLPRO, version 2008.1, a package of ab initio programs; University College Cardiff Consultants Limited : Cardiff, U.K., 2008; <http://www.molpro.net>.

(54) Hess, B.; Kutzner, C.; van der Spoel, D.; Lindahl, E. GRO-MACS 4: Algorithms for highly efficient, load-balanced, and scalable molecular simulation. *J. Chem. Theory Comput.* **2008**, *4*, 435–447.

(55) Jorgensen, W. L.; Tirado-Rives, J. The Opls Potential Functions for Proteins - Energy Minimizations for Crystals of Cyclic-Peptides and Crambin. *J. Am. Chem. Soc.* **1988**, *110*, 1657–1666.

(56) Gagliardi, L.; Orlandi, G.; Molina, V.; Malmqvist, P.-A.; Roos, B. Theoretical Study of the Lowest 1BU States of trans-Stilbene. *J. Phys. Chem. A* **2002**, *106*, 7355–7361.

(57) Quenneville, J.; Martinez, T. J. Ab initio study of cis-trans photoisomerization in stilbene and ethylene. *J. Phys. Chem. A* **2003**, *107*, 829–837.

(58) Improtà, R.; Santoro, F. Excited-State Behavior of trans and cis Isomers of Stilbene and Stiff Stilbene: A TD-DFT Study. *J. Phys. Chem. A* **2005**, *109*, 10058–10067.

(59) Celani, P.; Garavelli, M.; Ottani, S.; Bernardi, F.; Robb, M. A.; Olivucci, M. Molecular “Trigger” for the Radiationless Deactivation of

Photoexcited Conjugated Hydrocarbons. *J. Am. Chem. Soc.* **1995**, *117*, 11584–11585.

(60) Garavelli, M.; Celani, P.; Bernardi, F.; Robb, M. A.; Olivucci, M. Force Fields for Ultrafast Photochemistry: The Reaction Path for all-trans-Hexa-1,3,5-triene. *J. Am. Chem. Soc.* **1997**, *119*, 11487–11494.

(61) Gonzalez-Luque, R.; Garavelli, M.; Bernardi, F.; Merchan, M.; Robb, M. A.; Olivucci, M. Computational evidence in favor of a two-state, two-mode model of the retinal chromophore photoisomerization. *Proc. Natl. Acad. Sci. U.S.A.* **2000**, *97*, 9379–9384.